

Anomalous thermodynamics in a mixed spin-1/2 and spin-1 hexagonal nanowire system

R. A. Pimenta,^{1,*} O. Rojas,^{1,†} and S. M. de Souza^{1,‡}

¹*Departamento de Física, Universidade Federal de Lavras,
Caixa Postal 3037, 37200-000, Lavras, MG, Brazil*

(Dated: August 5, 2021)

The mixed spin-1/2 Ising model and spin-1 Blume-Capel model in an hexagonal nanowire structure under the presence of crystal field is considered. The free energy is obtained through the transfer matrix technique, which is solved numerically. Our main result lies in the presence of pseudo-transition in low temperature region near the ferrimagnetic/ferromagnetic boundary, due to the influence of a crystal field. The evidence of a pseudo-transition is observed in several quantities. Free energy first derivative quantities like entropy and internal energy show an abrupt but continuous jump, whereas quantities associated with second derivatives of the free energy like the specific heat exhibit a strong sharp peak, quite similar to a second order phase transition. We also investigate magnetization patterns and do not find evidence of spontaneous magnetization. Nevertheless, assuming a small magnetic field, we can induce a magnetization which resembles a spontaneous magnetization at a pseudo-critical temperature.

PACS numbers:

Keywords: Hexagonal nanowire, Blume-Capel, Ising, mixed-spin, pseudo-transition

I. INTRODUCTION

Recently, the magnetic properties of cylindrical nanowires have shown great potential applications such as magnetic recording, shift registers and logic gates, among other possible candidates. Indeed, over the last decades, several researches have been devoted to examine the magnetic and thermodynamic properties of nanowire systems, both experimentally [1–6] and theoretically [7–18].

From the theoretical point of view, several techniques have been used, such as mean-field approximation (MFA) [8, 18], effective field theory (EFT) [7, 13, 14], Monte Carlo simulation (MC) [18–20], among others [21, 22]. Special attention has been given to the study of mixed spin systems, in particular those composed by spin-1 and spin-1/2 particles arranged in hexagonal structures [7, 8, 14, 15, 18]. These works have predicted the occurrence of first and second order phase transitions as well as spontaneous magnetization at finite temperature. Such findings are astonishing, since these models do not violate the conditions of the non-existence theorem for phase transitions in one-dimensional systems with short range interactions, see *e.g.* [23] and references therein. Here the non-existence of phase transitions follows from the Perron-Frobenius theorem [24, 25] when applied to the associated transfer matrix [26]. Therefore, it is clear that one must be careful in drawing conclusions from approximative methods for such systems. Very recently, for example, the failure of EFT to predict phase tran-

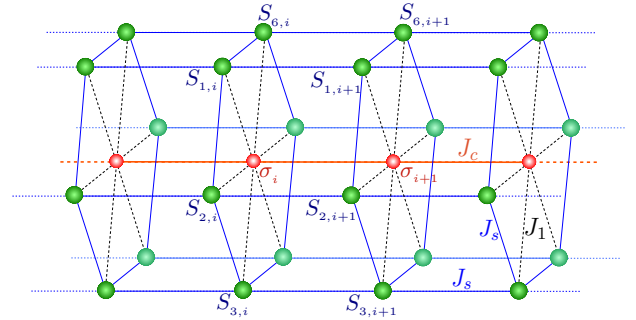


Figure 1: Mixed magnetic nanowire with spin 1/2 Ising in the central column and spin 1 Blume-Capel in the external hexagonal layer.

sitions in zero-dimensional and one-dimensional models has been thoroughly discussed in reference [27].

Nevertheless, peculiar anomalous behavior in thermodynamic quantities which resembles phase transition has been observed in a variety of 1D models, such as the Ising-Heisenberg spin model on a triangular tube [28], the diamond chain structure [29–32], the tetrahedral chain [33, 34] and even in a genuine one-dimensional Potts model [35]. The anomalous behavior has been called a pseudo-transition [36] and it is characterized by a continuous steep change (quite similar to a discontinuity) in the first derivatives of the free energy and by a giant peak (very similar to a singularity) in its second derivatives. Even so, according to the Perron-Frobenius theorem [24, 25], these one-dimensional models do not contradict the non-existence phase transition theorem since the transfer matrix elements are strictly positive.

Within in this context, we were motivated to analyze a 1D model in a hexagonal structure using the transfer matrix technique, which provides exact numerical results.

*Electronic address: pimenta@ifsc.usp.br

†Electronic address: ors@ufla.br

‡Electronic address: sergiomartinsde@ufla.br

Precisely, we investigate rigorously a mixed hexagonal Ising type nanowire system, composed by spin-1/2 particles in the core and spin-1 particles in the shell, previously considered in references [7, 8, 18], see fig.1. For this nanowire system it has been conjectured the existence of a possible first and second order type phase transitions, as well as possible spontaneous magnetization for certain values of the model parameters. As expected, the results from the transfer matrix approach do not confirm this conjecture. However, we do find a quite anomalous thermodynamic behavior.

Let us recall that the powerfulness of the transfer matrix approach for 1D systems relies in the fact that it allows to extract physical information in the thermodynamic limit from a finite sized matrix. However, for the model depicted in fig.1 the transfer matrix is huge, with dimension 1458×1458 . This is probably the reason why this approach has not yet been used, to the best of our knowledge, to study 1D nanowire systems. In fact, closed solutions are out of range and even numerical studies are computationally demanding. Even with good computing resources but using standard numerical programming languages such as Fortran, C++, Python, and other numerical computing software, they are usually limited to 15-18 decimal digits of precision, making the transfer matrix technique non-attractive. Moreover, especially in low-temperature regions, performing a high-precision numerical computation is hardly feasible using these languages. Consequently, obtaining physical quantities involving free energy derivatives becomes challenging because a naive analysis might induce us to a spurious outcome. In this sense, to get the maximum power of the numerical transfer matrix approach, we need a high precision numerical computation far beyond the 15-18 decimal significant precision. Hence, we use computer algebra systems like `Mathematica` and `Maple`, which provides arbitrary digits precision according to demand; typically, we use up to 50 digits or more. Indeed, this result is enough to perform any numerical derivatives of free energy with confidence avoiding misleading conclusions.

The use of high precision numerics allowed us a careful analysis of the anomalous behavior in various thermodynamic quantities in the nanowire model. For example, we do observe abrupt changes in the internal energy, entropy and magnetic quadrupole. On the other hand, we observe sharp peaks in the specific heat and correlation length. Indeed, a naive analysis could induce us to affirm a truly phase transition. However, once the thermodynamics is analyzed with magnifying glass, one concludes that this anomalous behavior is nothing else than a pseudo-transition observed previously in [36]. The pseudo-transition occurs near a ferrimagnetic (or core-ferromagnetic) and ferromagnetic quasi-phase boundary.

Let us remark that while the pseudo-transition can be visually observed in several thermodynamic quantities, the precise determination of the quasi-phase boundary is a delicate issue since there is no truly phase transition. For example, in a true phase transition, there is a diver-

gence in the specific heat and correlation length at a well defined critical temperature. In the present model, there is no singularity in these quantities, although the peaks are sharp and high. Within this limitation, we determine the temperatures where the peaks in the third largest eigenvalue of the transfer matrix (linked to the correlation function), T_p , and the specific heat, $T_{p'}$, occur, and also the temperature where a simple and interesting relation is satisfied by the eigenvalues of the transfer matrix, T_0 . We propose that the quasi-phase boundary is determined by the condition $T_0 \approx T_p \approx T_{p'}$.

This paper is organized as follows. In Section II, we define the nanowire Hamiltonian and analyze its ground state phase diagram. Next, in Section III, we introduce the transfer matrix, and carefully analyze its eigenvalues behavior. In Section IV we present the various thermodynamic quantities obtained from the numerical diagonalization of the transfer matrix, and discuss the quasi-phases of the system. In V we present the conclusions. In the appendix A, we make some considerations about the numeric derivatives.

II. NANOWIRE HAMILTONIAN

The nanowire model we consider is a mixed spin system composed of an Ising spin 1/2 (red circles) coupled to Blume-Capel spin-1 (green circles) per unit cell, see fig.1. The system can be described by the following Hamiltonian,

$$H = \sum_{i=1}^N H_{i,i+1}, \quad (1)$$

with

$$H_{i,i+1} = - \sum_{j=1}^6 [J_1 S_{j,i} \sigma_i + J_s (S_{j,i} S_{j,i+1} + S_{j,i} S_{j+1,i})] - J_c \sigma_i \sigma_{i+1} - \sum_{j=1}^6 (D S_{j,i}^2 + h_s S_{j,i}) - h_c \sigma_i, \quad (2)$$

where $\sigma_i \in \{-\frac{1}{2}, \frac{1}{2}\}$ and $S_{j,i} \in \{-1, 0, 1\}$ are the spins at the lattice site i with j marking the position in the i -th hexagon, and we assume periodic boundary conditions. The coupling constants are J_1 between Ising and Blume-Capel spins, J_c between Ising spins and J_s between Blume-Capel spins, D denotes the single-ion anisotropy or crystal field parameter of Blume-Capel spins, and h_c and h_s are external magnetic fields.

A. Zero temperature phase diagram

In this section, we examine the phase diagram of the Hamiltonian (2) at zero temperature. Since there are many free parameters in (2), we expect that the phase

diagram of model has a rich structure. Motivated by results obtained using the mean field approximation [8], we analyze the model around the crystal field value $D = -2.5$. In this work, for simplicity, we fix part of the set of parameters to be $J_1 = J_s = J_c = 1$, according to [8].

In fact, the work [8] predicts the existence of first-order phase transition at finite temperature around $D = -2.5$. This foretold first-order phase transition supposedly emerges as a consequence of the phase transition occurring at zero temperature. Therefore, we focus our attention on the vicinity of the zero-temperature phase transition. We consider the cases $D < -2.5$, $D = -2.5$ and $D > -2.5$, with and without magnetic fields. The phase diagrams, as function of D , h_c and h_s , are depicted in fig.2.

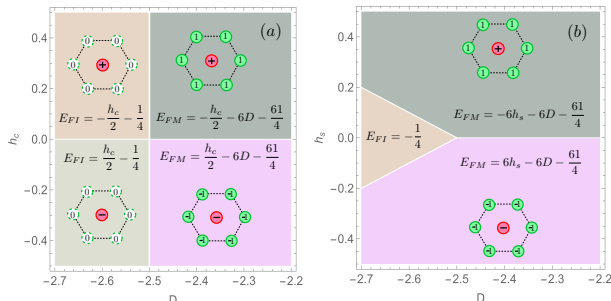


Figure 2: Ground state phase diagram at zero temperature. (a) $h_c \times D$ for $h_s = 0$. (b) $h_s \times D$ for $h_c = 0$.

For $D < -2.5$ and null magnetic fields $h_c = h_s = 0$, the corresponding ground state is aligned with all null shell spins, whereas the core spins are all aligned upwards or downwards, setting a ferrimagnetic state (|FI>),

$$|FI\rangle = \prod_{i=1}^N |0, 0, 0, 0, 0, 0\rangle_i \otimes |\sigma\rangle_i, \quad (3)$$

with corresponding ground state energy

$$E_{FI} = -\frac{1}{4}, \quad (4)$$

so that the system will be doubly degenerate with $\sigma = \pm 1/2$. Since the system is strictly in the null magnetic fields, we have the corresponding shell-spin magnetizations per unit cell $m_s = -\frac{1}{6} \frac{\partial E_{FI}}{\partial h_s} = 0$ and core-spin magnetization $m_c = -\frac{\partial E_{FI}}{\partial h_c} = 0$.

For $D > -2.5$ and strictly null magnetic field $h_c = h_s = 0$, the system is in the ferromagnetic (FM) phase and ground state energy is given by

$$E_{FM} = -\frac{61}{4} - 6D. \quad (5)$$

Similarly to our previous argument, the corresponding ground state can be expressed as follows,

$$|FM\rangle = \prod_{i=1}^N |S, S, S, S, S, S\rangle_i \otimes |\sigma\rangle_i, \quad (6)$$

where $S = 1$ and $\sigma = 1/2$ or $S = -1$ and $\sigma = -1/2$. Both core and shell spins are fully parallel to each other, and each of them doubly degenerates; therefore, the corresponding magnetizations become $m_s = -\frac{1}{6} \frac{\partial E_{FM}}{\partial h_s} = 0$ and $m_c = -\frac{\partial E_{FM}}{\partial h_c} = 0$.

For $D = -2.5$ and null magnetic fields ($h_c = h_s = 0$) the ground state energy on the boundary is four-fold degenerate and its is given by $E_b = -1/4$, with magnetizations $m_c = m_s = 0$.

We now analyze the effect of the magnetic fields h_c and h_s , according to fig.2, panels (a) and (b) respectively.

For $D < -2.5$, by turning on the external magnetic field (h_c), see fig.2-(a), the ground state energy will become,

$$E_{FI} = \begin{cases} -\frac{1}{4} - \frac{1}{2}h_c, & h_c > 0 \\ -\frac{1}{4} + \frac{1}{2}h_c, & h_c < 0 \end{cases}, \quad (7)$$

which implies that the system immediately raises its degeneracy by aligning itself with the magnetic field h_c ; thus, the core-spin magnetization per unit cell leads to $m_c = -\frac{\partial E_{FI}}{\partial h_c} = 1/2$ for $h_c > 0$ and $m_c = -1/2$ for $h_c < 0$. Nevertheless, we must be careful when taking $h_c \rightarrow 0$, which apparently leads us to a different nonzero magnetization, contradicting the magnetization with a strictly null magnetic field. Further details on this issue will be discussed later when we examine the thermal excitation.

For $D > -2.5$, fig.2-(a), when we consider the external magnetic field $h_c \neq 0$, the ground state energy is given by,

$$E_{FM} = \begin{cases} -\frac{61}{4} - 6D - \frac{1}{2}h_c, & h_c > 0 \\ -\frac{61}{4} - 6D + \frac{1}{2}h_c, & h_c < 0 \end{cases}, \quad (8)$$

and it follows that the corresponding magnetization will be $m_c = \pm 1/2$.

Now let us consider the effect of the field h_s , fig.2-(b). Inside the triangle $D + h_s \leq -2.5, D - h_s \leq -2.5$ the system is a ferrimagnetic state with ground state energy,

$$E_{FI} = -\frac{1}{4}, \quad D + h_s \leq -2.5, D - h_s \leq -2.5, \quad (9)$$

and we have $m_c = m_s = 0$. Outside the triangle, the degeneracy is lifted and the ground state energy is given by,

$$E_{FM} = \begin{cases} -\frac{61}{4} - 6D - 6h_s, & h_s > 0, D + h_s > -2.5 \\ -\frac{61}{4} - 6D + 6h_s, & h_s < 0, D - h_s > -2.5 \end{cases}, \quad (10)$$

leading to the magnetization per unit cell $m_s = \frac{1}{6}(\pm 6) = \pm 1$ and $m_c = 0$.

Let us mention that one can turn on both fields h_c and h_s and find interesting phase diagram. This point will be investigated elsewhere.

III. NANOWIRE TRANSFER MATRIX

The transfer matrix technique is the main tool to find rigorous exact results from the algebraic and numerical points of view. It has been widely used since almost a century ago to obtain exact results mainly in one and two two-dimensional lattices. Here we resort to this technique to investigate the free energy of the nanowire model. Our principal task is to solve the eigenvalues of transfer matrix \mathbf{V} with elements,

$$\langle \sigma, \{S_i\} | \mathbf{V} | \{S'_i\}, \sigma' \rangle = e^{-H_{i,i+1}/k_B T}, \quad (11)$$

where $\{S_i\}$ denotes $\{S_1, S_2, S_3, S_4, S_5, S_6\}$. The full transfer matrix of the model given by (2) has dimension 1458×1458 .

In order to solve the transfer matrix more handily, we use the cylindric symmetry C_{6v} on the shell spins (composed by spin-1 particles). The system is invariant under the rotation in $2\pi/6$ radians, so we have

$$\mathbf{C}_6 |S_1, S_2, S_3, S_4, S_5, S_6\rangle = |S_2, S_3, S_4, S_5, S_6, S_1\rangle, \quad (12)$$

where the cyclic group $\mathbf{C}_6 \mapsto \{I, \mathbf{C}_6, \mathbf{C}_6^2, \dots, \mathbf{C}_6^5\}$. The system is also invariant under reflection plane containing the rotational nanowire axis, so we have

$$\sigma_v |S_1, S_2, S_3, S_4, S_5, S_6\rangle = |S_6, S_5, S_4, S_3, S_2, S_1\rangle, \quad (13)$$

where $\sigma_v \mapsto \{I, \sigma_v\}$.

Therefore, taking into account the C_{6v} symmetry of the hexagonal nanowire, we can express the spin-1 particles in the nanowire shell by a matrix with dimension 729×729 which can be decomposed as a set of 12 sub-block irreducible matrices, as described below

$$3^6 = 92 \oplus 89 \oplus 86 \oplus 3(\oplus 80) \oplus 6(\oplus 37). \quad (14)$$

By $n(\oplus v)$ we mean $\oplus v$ is repeated n times. Including the core spin, the transfer matrix dimension doubles, and the block irreducible matrices dimension becomes as follows

$$3^6 \otimes 2 = 184 \oplus 178 \oplus 172 \oplus 3(\oplus 160) \oplus 6(\oplus 74). \quad (15)$$

As a result, we are able to express the transfer matrix of dimension 1458×1458 into 12 irreducible block matrices. We observe that the largest eigenvalue of the transfer matrix comes from the largest block matrix (184×184). We can even use the spin inversion symmetry in the absence of a magnetic field, so the largest matrix may still shrink to 92×92 . Here, however, we do not use this symmetry since we need a non-null magnetic field in order to analyze the magnetization.

Before considering the thermodynamic properties, let us check some properties of the transfer matrix eigenvalues. Let $\{\lambda_1, \lambda_2, \dots, \lambda_{1458}\}$ denote the 1458 eigenvalues of the transfer matrix. In addition, let us define for convenience the normalized eigenvalues $\hat{\lambda}_n = \lambda_n e^{-e_0/T}$, where e_0 is the ground state energy.

In fig.3 we illustrate the four largest eigenvalues around the field $D_c = -2.5$ where the zero temperature phase transition occurs. In panel (a) it is depicted the four largest eigenvalues considering a fixed temperature $T = 0.5$. We can observe that the curves $\hat{\lambda}_1$ and $\hat{\lambda}_3$ almost intersect for a given field D_p in the interval $-2.48 < D < -2.47$. Also, we notice that for $D < D_p$ the eigenvalues $\hat{\lambda}_2$ and $\hat{\lambda}_3$ are quasi degenerate, while for $D > D_p$ the eigenvalues $\hat{\lambda}_1$ and $\hat{\lambda}_2$ becomes quasi degenerate. At the same time, we observe that $\hat{\lambda}_4$ is significantly smaller than the other three eigenvalues.

In fig.3-(b), we plot the four largest normalized eigenvalues for the lower temperature $T = 0.4$. In this case, the curves do seem to intersect at a given critical field D_p . Here, the curves $\hat{\lambda}_1$ and $\hat{\lambda}_3$ seems to form a continuous decreasing function which intersects with $\hat{\lambda}_2$. This feature seems to point out to a phase transition at this point where $\hat{\lambda}_1$, $\hat{\lambda}_2$ and $\hat{\lambda}_3$ becomes almost the same for a particular value of parameter D . Nevertheless, using high precision numerics, we can zoom in around this region and observe actually a behavior similar to that depicted in panel (a), that is, all curves are smooth.

We reserve panels (c) and (d) in fig.3 to analyze the behavior of the four largest eigenvalues as a function of the temperature for fixed values of D . In panel (c), we fix $D = -2.475$, and observe that the curves $\hat{\lambda}_1$, $\hat{\lambda}_2$ and $\hat{\lambda}_3$ tend to intersect at a ‘‘critical’’ value $T_p \sim 0.48$. Similarly, in panel (d), we consider the four largest eigenvalues as a function of the temperature for fixed $D = -2.495$. That is, we get closer to the zero temperature critical value $D_c = -2.5$. Here, virtually, the curves appear to intersect. As before, the curves $\hat{\lambda}_1$ and $\hat{\lambda}_3$ appear to form a continuous function which is cut by $\hat{\lambda}_2$. Nevertheless, the curves never cross, as high precision numerics indicate.

Our high precision numerical results show that the largest eigenvalue of the transfer matrix is non-degenerate, as expected the Perron-Frobenius theorem [24, 25]. Further analysis of transfer matrix eigenvalues will be given in the next subsection.

A. Scaled eigenvalues behavior

Recall that the matrix elements of the transfer matrix (11) are Boltzmann weights, that is, they are strictly positive for finite non-null temperature. It follows from the Perron-Frobenius theorem [24, 25] that the largest eigenvalue of the transfer matrix is positive and non-degenerate. In addition to this important fact, the deeper study of the transfer matrix eigenvalues provides other crucial information about the physics of the system, see

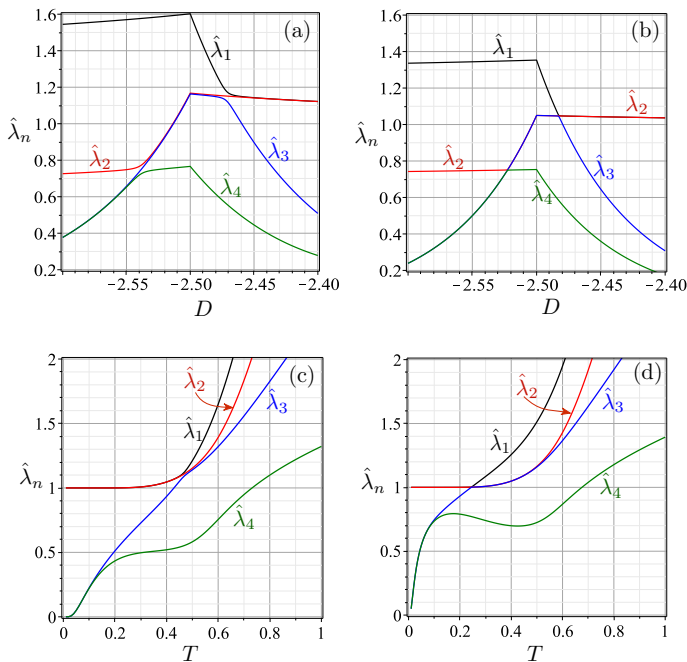


Figure 3: Transfer matrix leading eigenvalues $\hat{\lambda}_n$ with $h_c = h_s = 0$. (a) For $\hat{\lambda}_n$ as a function of D , assuming fixed $T = 0.5$. (b) For $\hat{\lambda}_n$ as a function of D , assuming fixed $T = 0.4$. (c) For $\hat{\lambda}_n$ as a function of T , assuming fixed $D = -2.495$. (d) For $\hat{\lambda}_n$ as a function of T , assuming fixed $D = -2.475$.

for instance reference [37].

In fact, as we argue in the following, certain properties of the transfer matrix eigenvalues can be used to characterize the boundaries between quasi-phases of the nanowire system. Indeed, the behavior of the scaled eigenvalues, defined by,

$$\Omega_n = \frac{\lambda_n}{\lambda_1}, \quad (16)$$

is particularly insightful for $n = 2, 3$. Our numerical results show that the behavior of the second and third largest eigenvalues is relevant in the vicinity of $D_c = -2.5$. For example, one can notice that the scaled eigenvalue have a strong peak $\Omega_3 \rightarrow 1$ around $D_c = -2.5$, although never really attains $\Omega_3 = 1$. This behavior is quite similar to that considered by Lavis [37] called an *incipient phase transition*, defined for finite size lattice.

In fig.4 we illustrate the scaled eigenvalues Ω_n as a function of the parameter D , for fixed temperatures, and as a function of T , for fixed values of D . The panel (a) reports the temperature $T = 0.5$, where we observe smooth curves, including a smooth peak in Ω_3 around $D = -2.48$. For $D \gtrsim -2.48$ we observe that the largest and second largest eigenvalues are quasi degenerate, *i.e.*, $\Omega_2 \rightarrow 1$. The third largest eigenvalue also plays an important role, that is, for a given parameter D and a given finite temperature, $\Omega_3 \rightarrow 1$ exhibits a maximum. Similarly, in

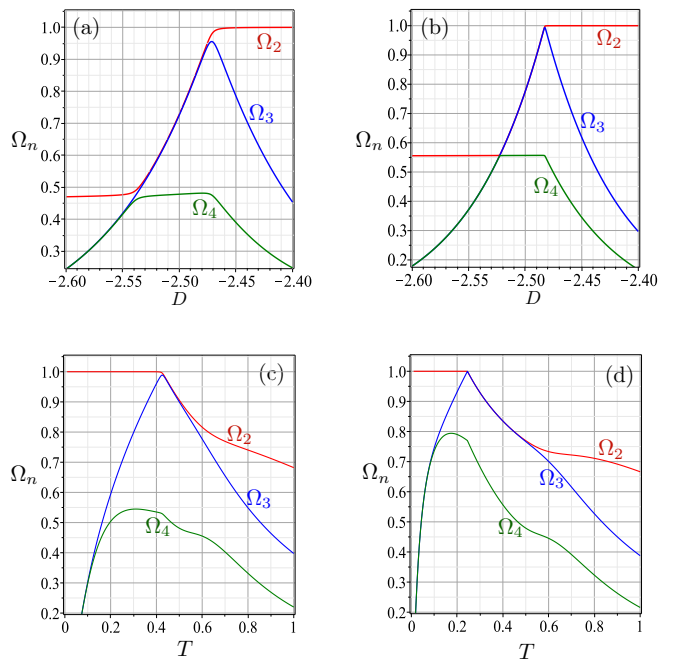


Figure 4: (a) Largest scaled eigenvalues Ω_n as a function of D with $h_c = h_s = 0$ for $T = 0.5$. (b) For $T = 0.4$. (c) Same quantities as a function of T assuming fixed $D = -2.48$. (d) For $D = -2.495$.

panel (b), we consider the scaled eigenvalues for a lower temperature $T = 0.4$. These curves get sharper, indicating presumably that there are crossing lines. However, the high-precision numerical calculation shows smooth curves similar to that shown in panel (a). These curves still behave sharper for lower temperatures, and by using standard numerical computation (like double-precision, providing 15 significant digits), we cannot distinguish the eigenvalues λ_1 and λ_2 . Naively, it may be inferred that the two largest eigenvalues are degenerate. However, high precision numerical computation gives us far beyond than 16 significant digits; we can in fact easily handle over 50 digits of precision using softwares like **Mathematica** or **Maple**, which clearly distinguishes the eigenvalues λ_1 and λ_2 , or λ_2 and λ_3 , as expected from the Perron-Frobenius theorem. In panel (c), we report the same quantity Ω_n as a function of temperature T assuming fixed $D = -2.48$. Here we observe the quasi-degeneracy between λ_1 and λ_2 roughly below the temperature of the peak of Ω_3 . Indeed we can verify that all curves are smooth and there is no degeneration between λ_1 and λ_2 . Likewise, in panel (d), we illustrate the eigenvalues for a fixed value of $D = -2.495$, and the curves become sharper. A careless analysis could induce the existence of crossing curves. However, a high-precision numerical result confirms that crossing curves are not present.

It is also interesting to observe the behavior of the scaled eigenvalues as a function of D and T , as depicted in fig.5. For Ω_2 , we can observe a plateau $\Omega_2 \sim 1$ for $D >$

-2.5 which only decays for relatively high temperatures. On the other hand, for $D < -2.5$ the decay occurs in the low temperature region. For Ω_3 , there is a very sharp region around $D_c = -2.5$ which, interestingly enough, marks the separation between quasi-phases, as we discuss below.

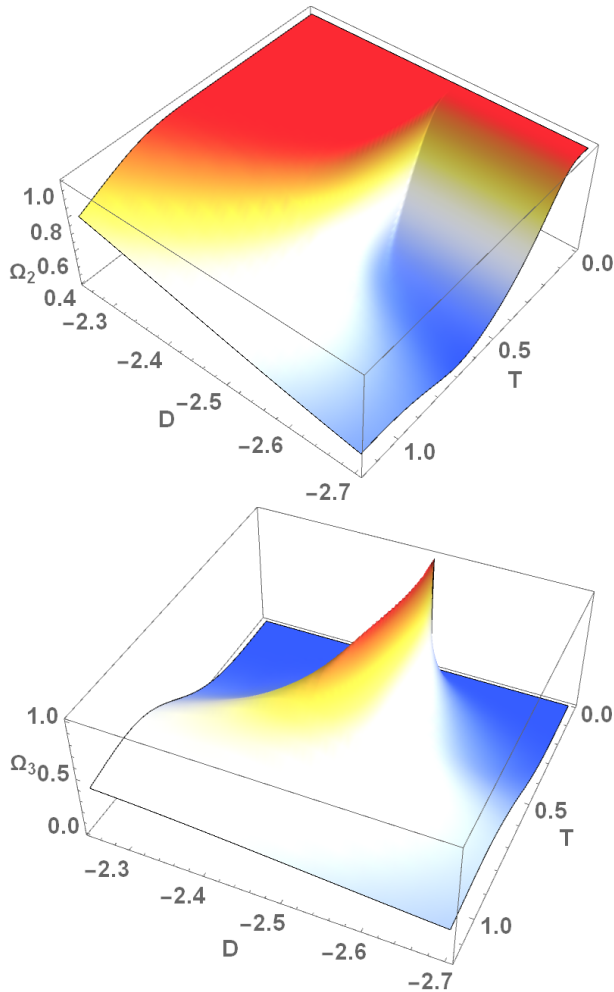


Figure 5: The scaled eigenvalues Ω_2 and Ω_3 as a function of D and T for $h_c = h_s = 0$.

In summary, we cannot expect any phase transition at finite temperature, neither first-order or second-order phase transition. However there is an anomalous behavior induced by the single-ion anisotropy around $D_c = -2.5$, which we will discuss below.

IV. NUMERICAL THERMODYNAMICS

In this section, we investigate numerically the dependence of the free energy on the model parameters, as well as its first derivatives (entropy, internal energy, magnetization, magnetic quadrupole) and second derivatives (specific heat, susceptibility). As before, for simplicity, we fix $J_1 = J_s = J_c = 1$.

A. Thermodynamic limit

Let us recall that, for a finite size chain (finite N), the partition function can be expressed using all 1458 eigenvalues of the transfer matrix, namely,

$$\mathcal{Z}_N = \sum_{k=1}^{1458} \lambda_k^N. \quad (17)$$

As a consequence, the free energy per unit cell can be expressed as follows

$$f_N = -T \ln(\lambda_1) - \frac{T}{N} \ln \left\{ 1 + \sum_{n=2}^{1458} \Omega_n^N \right\}, \quad (18)$$

where Ω_n is defined by (16) and T is the temperature in units of the Boltzmann constant.

All physical quantities will be analyzed in the thermodynamic limit. Since $\Omega_n < 1$ for all $n > 1$, the free energy in thermodynamic limit ($N \rightarrow \infty$) is given by,

$$f = -T \ln(\lambda_1). \quad (19)$$

The equation (19) means that the largest eigenvalue of the transfer matrix (which is a finite size matrix) captures the physics of the system in the thermodynamic limit.

Notice that although Ω_2 and Ω_3 are irrelevant within the thermodynamic limit, these scaled eigenvalues are important for the understanding of certain anomalies in the physical quantities. For example, the peaks in the scaled eigenvalue Ω_3 can be used to characterize a pseudo-critical temperature transition.

B. Free energy, entropy, internal energy and specific heat

We start by considering the behavior of the free energy and its derivatives in the temperature range $0.1 < T < 10$ with zero fields $h_c = h_s = 0$ and various single-ion fields D , namely, $D = -2.499, -2.495, -2.491, -2.487, -2.483, -2.480$. Numeric derivatives strategy is discussed in detail in appendix A. The obtained results are shown in fig.6. In panel (a), the free energy is depicted, and we can note that as one approaches $D_c = -2.5$, the free energy appears to have a ‘‘corner’’ around a given temperature. This ‘‘corner’’ smooths out as the field D increases, and the bending of the curve occurs in higher temperatures. The apparent corner in the free energy is reflected in abrupt (but continuous) changes in the entropy, see panel (b), and internal energy, see panel (c), as well as by the sharp and high peaks of the specific heat, see panel (d). The discontinuity in the first and divergence in the second derivatives, however, are in fact only apparent. Indeed, by zooming in very close the regions of abrupt changes, we do notice that all functions are continuous. As example, highlights for the field $D = -2.499$ are shown in fig.6.

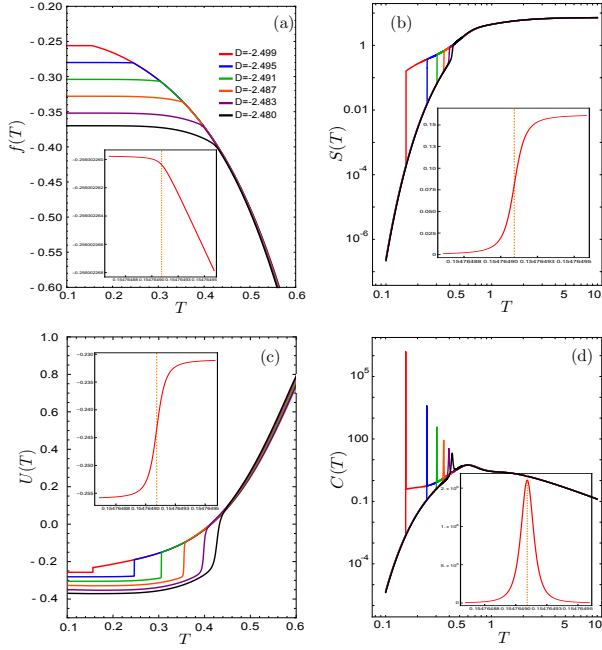


Figure 6: Thermodynamic quantities at zero fields $h_s = h_c = 0$ for $0.1 < T < 10$. (a) Free energy. (b) Entropy. (c) Internal energy. (d) Specific heat. The free and internal energies are shown in a smaller range where they are visually distinguishable for different values of D .

It is worth looking at the entropy as a function of D and T . The entropy surface is shown in fig.7. One can observe that there is a apparent jump (discontinuity) in the entropy value around $D_c = -2.5$ separating the FI and FM phases. Since there is no truly finite temperature phase transitions we define these regions by quasi-phases qFI and qFM [30, 33, 36]. The quasi-phases reflect the transition between the ferrimagnetic/ferromagnetic phases at zero-temperature. Observe that, obviously, there is no residual entropy for both quasi-phases. But what about residual entropy at the boundary of the two phases? We can verify that there is no residual entropy at the interface because the system is only doubly degenerate, and there is no macroscopic degeneration. When the residual entropy at the phase boundary is null, it is possible to observe an anomalous behavior at the phase boundary [38], characterizing the pseudo-critical temperature.

C. Correlation function

As we discussed in Sec. III-a, the largest and the second largest eigenvalues are quasi degenerate in the low temperature region. Recall that the two point correlation

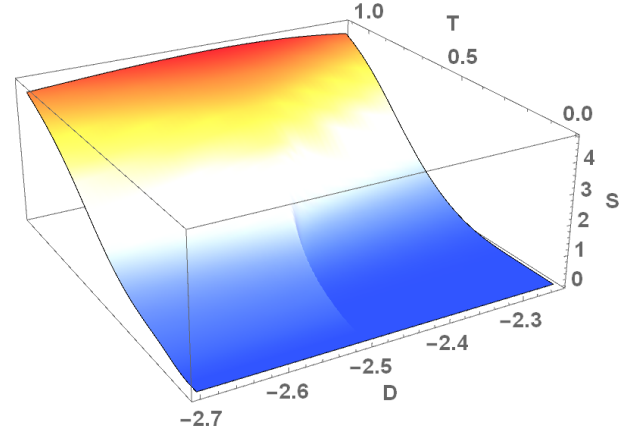


Figure 7: Entropy as a function of D and T for zero fields $h_c = h_s = 0$.

function can be expressed in general as follows,

$$\begin{aligned}
 \langle O_1 O_r \rangle &= \frac{\langle \psi | O_1 V^{r-1} O_r | \psi \rangle}{\lambda_1^{r+1}} \\
 &= \langle O_1 \rangle \langle O_r \rangle + \sum_{n=2}^{1458} \underbrace{\frac{\langle \psi | O_1 | \psi \rangle \langle \psi | V^{r-1} O_r | \psi \rangle}{\lambda_1 \lambda_n}}_{M_n} \Omega_n^r \\
 &= \langle O_1 \rangle \langle O_r \rangle + \sum_{n=2}^{1458} M_n e^{-r/\xi_n}, \quad (20)
 \end{aligned}$$

where the correlation length ξ_n is given by

$$\xi_n = -\frac{1}{\ln \Omega_n}. \quad (21)$$

In fig.8 we plot the scaled eigenvalues Ω_2 and Ω_3 as well as the correlations ξ_2 and ξ_3 as functions of the temperature for different values of D . In panel (a), we confirm the quasi degeneracy of the largest and second largest eigenvalues (that is, $\Omega_2 \rightarrow 1$) below a given temperature. This is reflected in huge values of the correlation $\xi_2(T)$, see panel (c). In panel (b), it is shown the scaled eigenvalue Ω_3 and we can observe the presence of well marked maximums $\Omega_3 \rightarrow 1$. This is reflected in huge peaks of $\xi_3(T)$, see panel (d). Despite the aggressive shapes, all curves are continuous. In fig.8-(d), the curve in dashed gray is formed by the correlation peaks obtained for various single-ion anisotropy D .

D. Quasi-phase and pseudo-critical temperature

The results of the previous subsections indicate the absence of first and second order phase transition for the nanowire model around $D_c = -2.5$, as expected from the non-existence theorem for phase transitions in one-dimensional systems with short range interactions [23]. Nevertheless, there is a remarkable thermodynamic behavior, as depicted, for example, in figs. 6 and 8. These

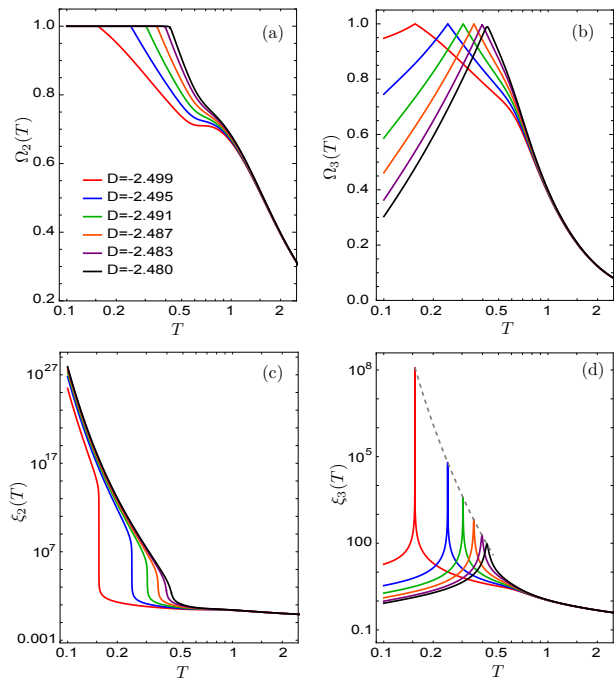


Figure 8: Ratios between the largest eigenvalues of the transfer matrix and associated correlation lengths for $h_c = h_s = 0$. The dashed curve in gray is formed by the peaks of the correlation length for various values of D . (a) $\Omega_2(T)$. (b) $\Omega_3(T)$. (c) $\xi_2(T)$. (d) $\xi_3(T)$.

peaks indicate the separation of two regions dominated by FI -type configuration and FM -type configuration, following the zero temperature pattern due to the thermal excitation in the low-temperature region. The quasi-phase boundary is well marked for temperature $T \lesssim 0.5$, whereas this boundary smoothly vanishes for higher temperatures.

This behavior is characteristic of a pseudo-phase transition, and it is interesting to determine the temperature where it occurs. One possibility is that the temperature where the pseudo-phase transition occurs can be determined from the peaks in correlation length ξ_3 or, equivalently, from the peaks in the scaled eigenvalue Ω_3 .

Let us now analyze the peaks of scaled eigenvalue Ω_3 , making the dependence on T and D explicitly. It is possible to find a peak at a given temperature by setting D and varying T . So, it is enough to analyze the maximum of $\Omega_3(T, D)$ as follows:

$$\left(\frac{\partial \Omega_3(T, D)}{\partial T} \right)_{T_p} = \Omega_{3, T_p} = 0, \quad (22)$$

Alternatively, fixing D we can find a temperature $T_{p'}$ where occurs the peak of specific heat $C(T, D)$ at $T_{p'}$, that is

$$\left(\frac{\partial C(T, D)}{\partial T} \right)_{T_{p'}} = C_{T_{p'}} = 0. \quad (23)$$

D	Eq.(22): T_p	Eq.(23): $T_{p'}$	Eq.(24): T_0
-2.499	0.1547649092435	0.1547649092435	0.1547649092435
-2.495	0.2451364474144	0.2451364476723	0.2451364543420
-2.491	0.3041836923345	0.3041837182997	0.3041850267111
-2.487	0.3535672004682	0.3535678022763	0.3536037505689
-2.483	0.3967956086305	0.3968065691948	0.3971636202687
-2.480	0.4255221428649	0.4255962726229	0.4268513697425
-2.470	0.4969631732231	0.4994220556277	0.5126192960524

Table I: Second column: peak temperature obtained from the ratio of eigenvalues T_p . Third column: peak temperature of specific heat. Fourth column: when eq.(24) is satisfied for a temperature T_0 , assuming $h_c = h_s = 0$.

Here we perform precise numeric derivatives following the information given in appendix A.

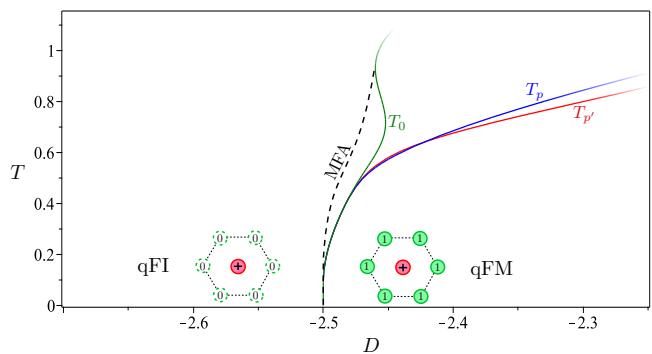


Figure 9: Pseudo-critical temperature T_p as a function of D , assuming zero magnetic field and fixed $J_1 = J_s = J_c = 1$, using the different conditions defined in (22) (blue curve), (23) (red curve) and (24) (green curve). The dashed line describes the MFA result [8].

Due to the absence of singularity, we cannot expect the sharp peaks of correlation length and specific heat to satisfy the relation $T_p = T_{p'}$, see fig.9. Although in the low-temperature region, we observe $T_{p'} \rightarrow T_p$, particularly for the parameters considered in fig.9, they are virtually indistinguishable up to $T \approx 0.5$. For higher temperatures, the peak for both quantities occurs at different temperatures assuming fixed D . For a more detailed comparison, we tabulated the highly accurate T_p and $T_{p'}$ in the second and third column of Table I, respectively. To find highly accurate $T_{p'}$ reported in Table I, we need over 30 significant decimal digits to perform precise numerical derivatives to obtain the specific heat, then localize the temperature at the sharp peak. In table I, for $D \lesssim -2.499$, both quantities are equal up to order 10^{-15} (not shown), as we display only the first 13 decimal digits. Whereas, for $D \gtrsim -2.495$, the peak temperatures differ in the tenth decimal digit. As soon as D increases, the differences become gradually increasing.

Additionally, from eigenvalues behavior discussed in

figs. 3 and 4, we can establish the following condition

$$1 + \Omega_3(T_0, D) = 2\Omega_2(T_0, D), \quad (24)$$

such that fixing D we can find a temperature T_0 that satisfy (24). The curve T_0 as a dependence of D is illustrated in fig. 9 by a green line. Again, we observe that $T_0 \rightarrow T_p$ in low-temperature regions is virtually identical up to $T \approx 0.5$, while T_0 behaves rather differently than T_p for higher temperatures. Similarly, in the fourth column of Table I, we observe in low-temperature region T_0 leads to T_p for $D \lesssim -2.499$, T_0 coincides with T_p up to 13 decimal digits, but when the crystal field D increases, the difference becomes gradually evident.

As we can see, it is hard to characterize the anomalous peak, which virtually looks like a genuine phase transition. In contrast, the peak is sharply pronounced, but it gradually becomes a rounded, broad peak as soon as D increases. We cannot establish a limit between sharp and broad peaks because the curves split slowly. A possible definition of pseudo-transition could be the condition $T_0 \approx T_p \approx T_{p'}$. In fig.9, this condition should occur at $T_p \approx 0.5$.

On the other hand, comparing with the “critical” temperature obtained from MFA [8, 18], which is depicted as a dashed line in fig.9, we observe that, effectively, at sufficiently low temperature below $T \approx 0.15$, the mean-field result looks the same as T_p . Still, for higher temperatures, the mean-field “critical” temperature deviates considerably from the pseudo-critical temperature.

In summary, we do not observe either first or second-order phase transition at a finite temperature, such as predicted in references [7, 8, 18]. Instead, we just observed the vestiges of zero-temperature phase transition between FI and FM phases at finite temperature. In general, there is an extra residual entropy in the interface at zero temperature, which is responsible for destroying any evidence of zero-temperature phase transition as soon as temperature increases. However, the phase boundary between FI and FM has a peculiar property, there is no residual entropy at the interface, or there is no extra entropy at the boundary [38]. Consequently, the zero-temperature phase transition vestiges survive at a relatively higher temperature.

E. Magnetization and susceptibility

So far, we have considered the thermodynamics for null magnetic fields $h_c = h_s = 0$. In this subsection, we investigate the dependence of the free energy with respect to the fields h_c and h_s . For simplicity, we fix $D = -2.480$ and temperatures below, above and at the pseudo-critical temperature $T_p = 0.4255221428649$.

We start by considering $h_s = 0$ and varying h_c , see fig. 10. The magnetization at given h_c and T can be computed as follows,

$$m_c(h_c) = -\frac{f(T, h_c + \delta h_c) - f(T, h_c - \delta h_c)}{2\delta h_c}, \quad (25)$$

where δh_c is a small step. Here we use $\delta h_c = 10^{-20}$ and perform the numerical calculations using 60 digits (see appendix A). In panel (a), we plot the dependence of free energy with respect to the core magnetic field h_c . For $T \leq T_p$, we observe an apparent corner at $h_c = 0$. This “corner”, similarly to our previous discussions, is only apparent, as we highlighted for the extreme case $T = T_p - 0.1$. The apparent corner leads to an abrupt change in the magnetization, as shown in panel (b). In fact, one can see that for temperatures $T < T_p$ (solid line), $T = T_p$ (tick line) and $T > T_p$ (dashed line) the magnetization vanishes smoothly for zero field $h_c = 0$. Therefore, there is no signal of spontaneous magnetization. To recall typical magnetization pictures, see *e.g.* [39]. Concerning the susceptibility, see panel (c), the strong changes in the free energy and magnetization reflects into a sharp peak for χ_c . Nevertheless, we can again zoom in very close to $h_c = 0$, and realize that in fact the susceptibility is a continuous function of h_c , even in the extreme case $T = T_p - 0.1$. It is important to remark that the free energy is a even function of h_c and the null magnetization at $h_c = 0$ is indeed a foreseen result.

Similar results are obtained by considering $h_c = 0$ and varying h_s , see fig.11.

The fact that approximative methods [8, 18] do predict a spontaneous magnetization deserves a deeper investigation from the perspective of the transfer matrix approach. In order to do that, we turn on a small field h_c , and compute numerically the magnetization around this point using a very small step $\delta h_c = 10^{-20}$, that is,

$$m_c(T) = -\frac{f(T, h_c + \delta h_c) - f(T, h_c - \delta h_c)}{2\delta h_c}, \quad (26)$$

for different initial fields h_c , and similarly the susceptibility. This means that we are slightly far from the “corner” in the free energy as a function of h_c . Similar calculation is done for h_s . For these calculations, we choose $D = -2.49$. In order to deal with the small step in the first and second derivatives, we use about 60-80 digits calculations (see appendix A). The results are shown in fig.12. In panel (a), we observe that the a small field $h_c = 10^{-12}$ is enough to induce a non-zero magnetization in the low-temperature region. Interestingly, for different small fields h_c , all curves seems to collapse as we approach the pseudo-critical temperature. This is confirmed by using a log-scale, see the bottom of panel (a), described by dotted line, where we observe a change of concavity at T_p , although in linear scale we cannot observe this effect. On the other hand, the magnetic susceptibility shows an apparent and remarkable peak at T_p for $h_c \sim 10^{-4} - 10^{-6}$, inducing us to believe that we are facing a truly phase transition at T_p , but this illusory peak vanishes for $h_c < 10^{-6}$, becoming only a substantial increase at T_p in the magnetic susceptibility. For the dashed line, we use the tiny value $h_c = 10^{-30}$, with a derivative step of $\delta h_c = 10^{-50}$ and perform the calculations using 200 digits. Clearly, the susceptibility leads to a divergence at $T = 0$ when $h_c \rightarrow 0$. A similar behavior

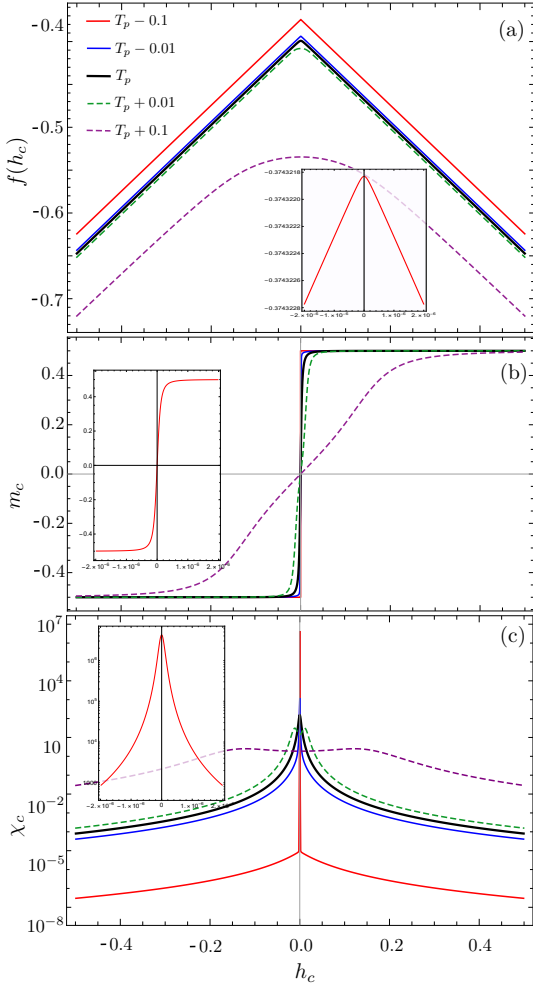


Figure 10: Free energy and its derivatives as functions of h_c for fixed $D = -2.480$. (a) Free energy. (b) Magnetization. (c) Susceptibility.

is observed for the magnetic field h_s of the shell spins, see panel (b).

It is worth remarking that the magnetization obtained from the transfer matrix technique behaves step-like function in temperature. In contrast, the MFA and MC [7, 8, 18] approaches report a rounder function quite similar to the magnetization of two-dimensional systems.

F. Magnetic quadrupole

We finally investigate the dependence of the magnetic quadrupole with respect to the temperature. The magnetic quadrupole is given by the derivative of the free energy with respect to the single-ion field D and the results are plotted in fig.13. Similarly to the previous thermodynamics quantities, we observe a steep change of the function $q(T)$ around the pseudo-critical temperature. As a matter of fact, when we zoom in close to T_p we observe a well behaved function, as enhanced for $D = -2.499$

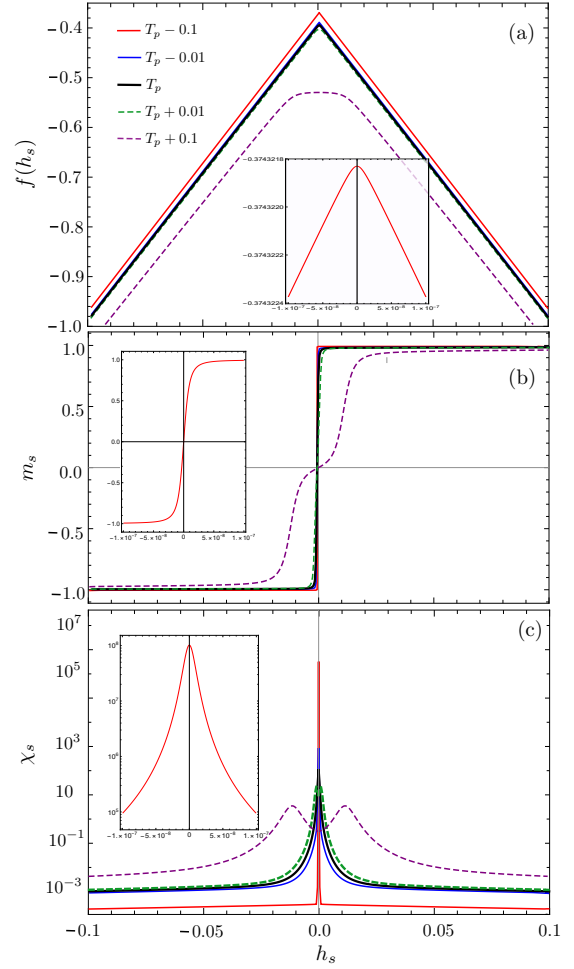


Figure 11: Free energy and its derivatives as functions of h_s for fixed $D = -2.480$. (a) Free energy. (b) Magnetization. (c) Susceptibility.

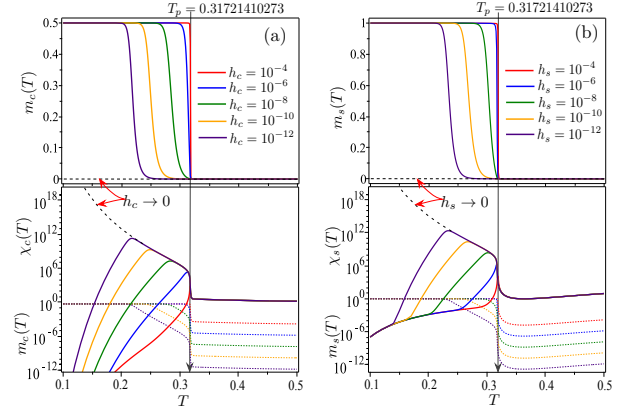


Figure 12: Magnetization in linear (top) and log (dotted, bottom) scale and susceptibility in log scale for different initial small fields and $\delta h_c = \delta h_s = 10^{-20}$. The dashed line in black corresponds to the field $h_c = 10^{-30}$. We use here $D = -2.49$.

in fig.13. Our results qualitatively look similar to that found in reference [8], although the critical temperature does not coincide.

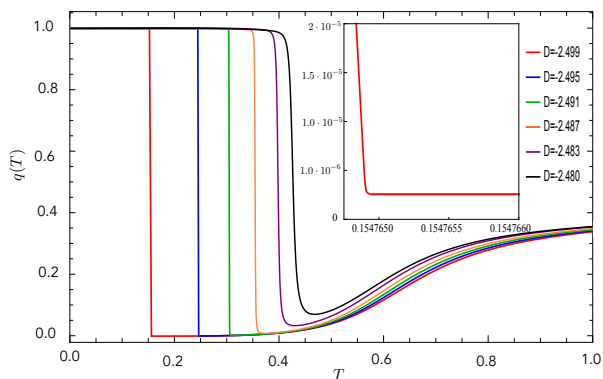


Figure 13: Magnetic quadrupole for various single-ion fields D and $h_c = h_s = 0$.

An interesting observation is that the magnetic quadrupole as a function of T and D presents a clear demarcation of the quasi-phases which we discussed previously, see fig.14. Definitely, the MFA result [8] deviates from sharp boundary marked by quasi-phases qFI and qFM.

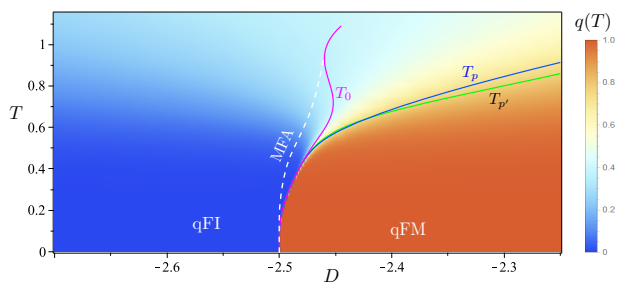


Figure 14: Magnetic quadrupole as a function of T and D for $h_c = h_s = 0$.

V. CONCLUSION

We have analyzed the thermodynamic behavior of the mixed spin-1/2 and spin-1 hexagonal nanowire system using exact numerical diagonalization of the transfer matrix. The results indicate the presence of a pseudo-transition, characterized by a steep change of first derivatives of the free energy and by sharp peaks in its second derivatives, around the pseudo-critical temperature, which we have computed for various values of the crystal field D . Nevertheless, by zooming in the thermodynamic quantities around the pseudo-critical temperature we observe that the discontinuities and divergences are only apparent, as expected. This phenomena is linked to the fact the largest eigenvalue of the transfer matrix is quasi-degenerate, which means that some of the Boltz-

mann weights of the transfer matrix are very tiny in the low-temperature region. In order to observe the non-degeneracy of the eigenvalues, we are required to use high precision numerics. Let us remark that we have considered a small piece of the model parameters manifold, close to the value $D = -2.5$ and null magnetic fields. It is certainly worth to investigate the thermodynamics beyond this region. The exact numerical diagonalization can be used to analyze other systems, for instance, a generalized version of the nanowire with spin- s_1 core and spin- s_2 shell. The limitation is the dimension of the associated transfer matrix.

Acknowledgments

RAP was supported by CNPq (grant # 150829/2020-5). OR and SMS thanks CNPq and FAPEMIG.

Appendix A: Numerical derivative significant digits

Performing numerical derivatives require thorough analysis, specially when we consider the low-temperature region.

In this work we are using centered formula with two points to perform the first order derivative. To get a reliable result, we take into account the error of numerical derivatives, see [40],

$$\left| 1 - \frac{\bar{f}'(x)}{f'(x)} \right| \lesssim p_1 \left\{ \frac{h^2}{6} + \frac{1}{h} \epsilon r_1 \right\}, \quad (\text{A1})$$

here $f'(x)$ is the first order derivative of $f(x)$, while

$$\bar{f}'(x) \equiv \frac{f(x+h) - f(x-h)}{2h}, \quad (\text{A2})$$

is the numeric derivative and

$$p_1 = \frac{|f'''(x)|}{|f'(x)|}, \quad r_1 = \frac{|f(x)|}{|f'''(x)|}, \quad (\text{A3})$$

and ϵ is the machine epsilon.

Basically, the root of this error lies in the truncation error proportional to h^2 and the round-off error proportional to h^{-1} ; this means that we cannot carry out $h \rightarrow 0$ as small as we want. Therefore, by minimizing the error the optimal value for h leads to the following relation

$$\epsilon = \frac{h^{*3}}{3r_1}. \quad (\text{A4})$$

At optimal h^* the relation (A1) becomes

$$\left| 1 - \frac{\bar{f}'(x)}{f'(x)} \right| \approx p_1 \left\{ \frac{h^{*2}}{6} + \frac{1}{h^*} \epsilon r_1 \right\} = \frac{p_1}{2} h^{*2}. \quad (\text{A5})$$

The significant digits of numerical derivative is defined by

$$n_o = -\log_{10} \left| 1 - \frac{\bar{f}'(x)}{f'(x)} \right|.$$

We can express $n_h = -\log_{10}(h^*)$, as a function of n_ϵ ($\epsilon = 10^{-n_\epsilon}$), obtaining,

$$n_h = \frac{1}{3}n_\epsilon - \frac{1}{3}\log_{10}(3r_1). \quad (\text{A6})$$

Typically r_1 should be of the order $r_1 \sim 1$, but when $r_1 \gg 1$, special attention needs to be taken when performing numerical derivatives with a double-precision number. This means that for a double-precision number, we have $n_\epsilon \sim 15$, so the optimal value of h^* should not be lower than $h^* \sim 10^{-5}$.

Rewriting eq.(A5), we have

$$n_o \approx 2n_h - \log_{10}\left(\frac{p_1}{2}\right). \quad (\text{A7})$$

As a consequence, the accuracy of the numerical differentiation could have no more than $n_o \lesssim 2n_\epsilon/3 \sim 10$ significant digits. Of course, one could improve this result by using more sophisticated numerical derivative, like centered formula with 4 or more points, but this is time consuming, and one would not go far than double precision number accuracy. Usually, p_1 is of order $p_1 \sim 1$, but in low-temperature regions, p_1 should be $p_1 \gg 1$. Accuracy might be even worse, making it difficult to obtain a precise result. The only possibility to improve the numerical derivative considerably is by increasing the significant decimal digits. For example, assuming $n_\epsilon \approx 30$, the corresponding optimal h^* should be of order $h^* \approx 10^{-10}$ with numerical precision of order $n_o \sim 15$ although this precision might be significantly lower than 15 digits for lower temperature.

A similar analysis may be done for the second order derivative. Here we use central formula with 3 points,

$$\left|1 - \frac{\bar{f}''(x)}{f''(x)}\right| \lesssim p_2 \left\{ \frac{h^2}{12} + \frac{1}{h^2}\epsilon r_2 \right\}, \quad (\text{A8})$$

here $f''(x)$ is the second order derivative of $f(x)$, while

$$\bar{f}''(x) \equiv \frac{f(x+h) - 2f(x) + f(x-h)}{h^2}, \quad (\text{A9})$$

is the numeric derivative with

$$p_2 = \frac{|f^{(iv)}(x)|}{|f'(x)|}, \quad r_2 = \frac{|f(x)|}{|f^{(iv)}(x)|}. \quad (\text{A10})$$

As we can see in (A8), h cannot be set arbitrarily small because of numerical precision ϵ . Instead, minimizing the

error of (A8) we have the optimal value,

$$\epsilon \approx \frac{h^{*4}}{36r_2}. \quad (\text{A11})$$

For the optimal h , the eq.(A8) results in

$$\left|1 - \frac{\bar{f}''(x)}{f''(x)}\right| \approx p_2 \left\{ \frac{h^2}{12} + \frac{1}{h^2}\epsilon r_2 \right\} = \frac{p_2}{9}h^{*2}. \quad (\text{A12})$$

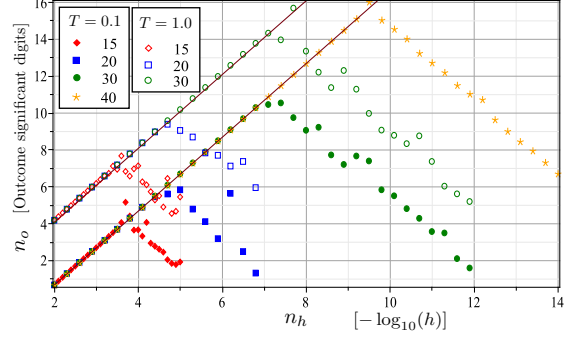


Figure 15: Significant digits n_o of specific heat as function of n_h , for $D = -2.499$ and null magnetic field. Upper solid line [$n_o \approx 2n_h + 0.1$] corresponds to $T = 1$, and lower solid line [$n_o \approx 2n_h - 3.3$] is given for $T = 0.1$.

Therefore, the precision of significant digits becomes

$$n_o \approx 2n_h - \log_{10}\left(\frac{p_2}{9}\right). \quad (\text{A13})$$

In order to illustrate the the significant digits n_o as a function of n_h , we show in fig.15 the accuracy of the specific heat assuming $D = -2.499$ and null magnetic fields. The upper solid line is given by $n_o \approx 2n_h + 0.1$, which corresponds to $T = 1$. Here p_2 can be obtained from fig. 15, which is of order $p_2 \sim 7.1$. In this case the double precision number $n_\epsilon \approx 15$ leads to an optimal significant digits $n_o \sim 7$ of specific heat, and by extending to $n_\epsilon \sim 20$ we get $n_o \sim 9$ significant digits, while for $n_\epsilon \sim 30$ we get $n_o \sim 14$. However, for the lower temperature $T = 0.1$, the solid line is given by $n_o \approx 2n_h - 3.3$, and the corresponding p_2 becomes $p_2 \sim 1.8 \times 10^4$. This factor influences significantly in the specific heat precision falling roughly in 3 significant digits. For lower temperatures the accuracy would decrease even more dramatically.

-
- [1] C. Bran, J. A. Fernandez-Roldan, R. P. del Real, A. Asenjo, O. Chubykalo-Fesenko and M. Vazquez, *Nanomaterials* **11**, 600 (2021)
 [2] A. Iorio, M. Rocci, L. Bours, M. Carrega, V. Zannier, L. Sorba, S. Roddaro, F. Giazotto, and E. Strambini, *Nano Lett.* **19**, 652 (2019)
 [3] K. Moon, J. Lee, S. Choe, K. Shin, *Current Applied*

- Physics* **9**, 1293 (2009)
 [4] A. Ghaddar, F. Gloaguen and J. Gieraltowski, *J. Phys.: Conf. Ser.* **200**, 072032 (2010)
 [5] M. U. Torres, A. Sitek, S. I. Erlingsson, G. Thorgilsson, V. Gudmundsson, and A. Manolescu, *Phys. Rev. B* **98**, 085419 (2018)
 [6] P. Wójcik, A. Bertoni, and G. Goldoni, *Phys. Rev. B*

- 103**, 085434 (2021)
- [7] E. Kantar, Y. Kocakaplan, *Solid State Commun.* **177**, 1 (2014)
- [8] R. G. B. Mendes, F. C. Sá Barreto, J. P. Santos, *Braz. J. of Phys.* **48**, 137 (2018)
- [9] O. Cankon, A. Erdinc, F. Taskin, A. F. Yildirim, *J. Magn. Mater.* **324**, 508 (2012)
- [10] M. Keskin, E. Kantar, *J. Supercond. Nov. Magn.* **30**, 1849 (2017)
- [11] B. Deviren, Y. Sener, *J. Magn. Mater.* **386**, 12 (2015)
- [12] N. Hachem, I.A. Badrour, A. El Antari, A. Lafhal, M. Madani, M. El Bouziani, *Chin. J. Phys.* **71**, 12 (2021)
- [13] Y. Kocakaplan and E. Kantar, *Eur. Phys. J. B* **87**, 135 (2014)
- [14] E. Kantar, *J. Supercond. Nov. Magn.* **28**, 2865 (2015)
- [15] E. Kantar, Y. Kocakaplan, *J. Magn. Mater.* **393**, 574 (2015)
- [16] B. Nmaila, K. Htoutou, L.B. Drissi, R. Ahl Laamara, *Solid State Communication*, **336**, 114418 (2021)
- [17] J. Holanda, *J. Phys. D: Appl. Phys.* **54**, 245004 (2021)
- [18] R.G.B. Mendes, F.C. Sá Barreto, J.P. Santos, *J. Magn. Mater.* **513**, 167150 (2020)
- [19] O. Iglesias, X. Batlle, A. Labarta, *Physical Review B* **72**, 212401 (2005)
- [20] M. Vasilakaki, K.N. Trohidou, *Physical Review B* **79**, 144402 (2009)
- [21] J. M. Wesselinowa, *J. Magn. Mater.* **322**, 234 (2010)
- [22] V. A. Tanriverdiyev, *J. Magn. Mater.* **393**, 188 (2015)
- [23] J. A. Cuesta and A. Sanchez, *Journal of Statistical Physics* **115**, 869 (2004).
- [24] F. Ninio, *Phys. A: Math. Gen.* **9**, 1281 (1976).
- [25] K. Y. Lin Chin. *Journ. Phys.* **15**, 283 (1977).
- [26] R. J. Baxter, *Exactly Solved Models in Statistical Mechanics* (Academic Press, 1989)
- [27] J. Strečka, K. Karl'ová, O. Krupnitska, *Phys. E: Low-Dimens. Syst. Nanostructures* **133**, 114805 (2021)
- [28] J. Strečka, R. C. Alecio, M. Lyra and O. Rojas, *J. Magn. Mater.* **409**, 124 (2016)
- [29] J. Strečka, *Acta Phys. Pol. A* **137**, 610 (2020)
- [30] O. Rojas, J. Strečka, M. L. Lyra, S. M. de Souza, *Phys. Rev. E* **99**, 042117 (2019).
- [31] O. Rojas, J. Torrico, L. M. Veríssimo, M. S. S. Pereira, S. M. de Souza and M. L. Lyra, *Phys. Rev. E* **103**, 042123 (2021)
- [32] T. Krokhmalkskii, T. Hutak, O. Rojas, S. M. de Souza, O. Derzhko, *J. Magn. Mater.* **573**, 125986 (2021)
- [33] O. Rojas, J. Strečka, O. Derzhko, S. M. de Souza, *Phys.: Condens. Matter* **32**, 035804 (2020)
- [34] L. Galisova and J. Strečka, *Phys. Rev. E* **91**, 022134 (2015)
- [35] Y. Panov and O. Rojas, *Phys. Rev. E* **103**, 062107 (2021)
- [36] S. M. de Souza and O. Rojas, *Solid State Commun.* **269**, 131 (2018)
- [37] D. A. Lavis, *Statistical Mechanics of Phase Transitions* (Springer Netherlands, 2015).
- [38] O. Rojas, *Braz. Journ. Phys.*, **50**, 675 (2020)
- [39] J. M. Yeomans, *Equilibrium Statistical Mechanics of Lattice Models* (Clarendon Press, 1992)
- [40] Knut Mørken, *Numerical Algorithms and Digital Representation* (2013)